Excitability in optically injected semiconductor lasers: Contrasting quantum-well- and quantum-dot-based devices

B. Kelleher,[1,2] C. Bonatto,[1,2] G. Huyet,[1,2] and S. P. Hegarty[2]
[1]*Centre for Applied Photonics and Process Analysis, Cork Institute of Technology, Cork, Ireland*
[2]*Tyndall National Institute, Lee Maltings, Cork, Ireland*
(Received 14 July 2010; published 24 February 2011)

Excitability is a generic prediction for an optically injected semiconductor laser. However, the details of the phenomenon differ depending on the type of device in question. For quantum-well lasers very complicated multipulse trajectories can be found, while for quantum-dot lasers the situation is much simpler. Experimental observations show the marked differences in the pulse shapes while theoretical considerations reveal the underlying mechanism responsible for the contrast, identifying the increased stability of quantum-dot lasers to perturbations as the root.

DOI: 10.1103/PhysRevE.83.026207 PACS number(s): 05.45.Xt, 42.60.Mi, 42.55.Px, 42.65.Sf

I. INTRODUCTION

Excitability refers to the response of a system to perturbations from a steady state. In an excitable system, perturbations below a certain threshold result in short phase-space trajectories back to the steady state. However, a perturbation above the threshold results in a large phase-space response as the system returns to the steady state. In the case of noise-induced excitability the noise within a system is sufficient to push it beyond the threshold and so excitable responses are spontaneously generated. The form of these responses depends on the system in question: examples include voltage spikes in the case of neuronal excitability, chemical concentration spikes in reaction-diffusion systems, and intensity pulses in semiconductor lasers (see [1] and references therein for studies of excitability in different areas of science). In this paper we consider the excitable dynamics observed with an optically injected semiconductor laser. In this configuration two lasers are coupled in a unidirectional manner so that light from one (the master) is injected into the cavity of the other (the slave). When the frequency of the master laser is sufficiently close to that of the slave and the coupling is sufficiently high, the field of the slave can become synchronized with that of the master. Other observed dynamics are chaos, multistability, and the focus of this paper, excitability. (See [2] for a review of optically injected quantum-well-based semiconductor lasers and [3–6] for recent results using quantum-dot lasers.) Excitability can also be observed in lasers with saturable absorbers [7], lasers undergoing optical feedback [8], multisection lasers [9], and ring lasers [10]. One particular benefit of the optically injected system is its amenability to analysis both experimentally and theoretically; indeed excellent quantitative agreement between experiment and theory is possible, as shown in [11].

The excitable regime for the case of optical injection is found for low levels of injection strength. A common assumption is that the Adler model [12] for the phase locking of two oscillators can explain the underlying physics in this regime. The Adler model is a prototype for excitability in phase-locked oscillators and is governed by the equation

$$\dot{\phi} = -\Delta - K \sin\phi, \tag{1}$$

where Δ is the detuning (the frequency of the master minus that of the slave), ϕ is the phase difference between the master and the slave, and K is a measure of the injection rate. Excitable events in this system consist of 2π rotations of the slave phase. The important realization that the Adler mechanism is not always the mechanism for excitability in optically injected semiconductor lasers was made in [13]. There it was shown that there are certain regions—homoclinic teeth—where the system is excitable but where very complicated excitable trajectories involving rotations of $2n\pi$ can be obtained. However, this was a numerical analysis of the system without an experimental confirmation of the phenomenon. Excitable pulses were observed experimentally using quantum-dot lasers operating at approximately 1300 nm in [3]. However, there was no indication of the complex multipulse behavior expected in homoclinic teeth. For single-mode devices, only single pulses were observed and in [4] it was shown that these corresponded to excitable phase slips of 2π rotations. Multipulse excitability in the form of double pulses (4π phase slips) was observed using multimode devices in [3] but appears to result from a period doubling of the single-pulse behavior rather than from a homoclinic tooth. Furthermore, it was shown in [14] that the same saddle-node mechanism gives rise to trains of pulses and phase slips in mutually coupled quantum-dot lasers.

In this work we reveal experimental multipulse excitability using quantum-well-based lasers and contrast this with the observations for quantum-dot-based lasers. We consider rate equation models for the two types of devices and examine the behavior via analytic calculations and numerical studies of the Lyapunov exponents and numerical time series. Via this analysis we show how the increased stability of quantum-dot lasers leads to a reduction in observed chaotic behavior and the consequent removal of the multipulse excitability, thus explaining the discrepant observations.

II. EXPERIMENTAL EXCITABLE BEHAVIOR

The experimental setup is shown in Fig. 1. Light from the master laser was coupled to the slave using a lensed fiber via an optical circulator (with an isolation greater than 40 dB). The light from the slave was then free-space-coupled to an oscilloscope of bandwidth 12 GHz. (An optical isolator with

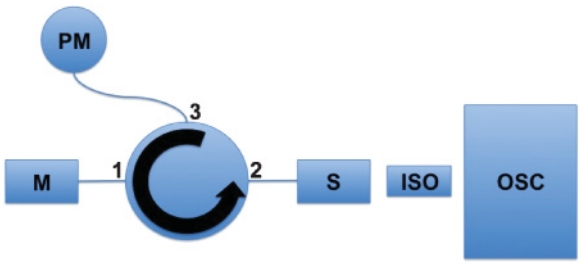

FIG. 1. (Color online) Experimental setup. M is the master laser, S is the slave laser, PM is a power meter used to measure the injection strength, OSC is a digital oscilloscope, and ISO is an optical isolator used to prevent unwanted feedback effects.

isolation greater than 40 dB was used to prevent unwanted feedback effects.) The master laser was a commercially available tunable laser with a linewidth of less than 100 kHz. The quantum-well slave laser was a single-mode device similar to those described in [15] and the quantum dot a single-mode (distributed feedback) device similar to those used in [4]. (Both types of device operated at a wavelength of around 1300 nm. The threshold of the quantum well device was 14 mA and that of the quantum-dot device was 38 mA and both were operated at approximately 1.5 times threshold.)

A. Negative detuning

Let us begin with the quantum well device. Close to the locking boundary for negative detuning, intensity pulsations such as those in Fig. 2 were observed. The injection strength

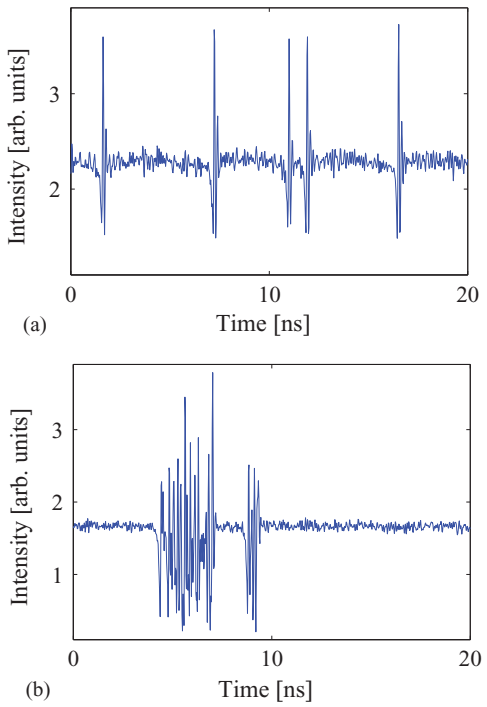

FIG. 2. (Color online) Experimental pulses for the quantum well device. (a) Single-pulse behavior and (b) multipulse behavior associated with a homoclinic tooth. For (a), the injection strength was approximately 0.05 and the detuning was approximately −1.5 GHz, while for (b), the injection strength was approximately 0.1 and the detuning was approximately −2.5 GHz.

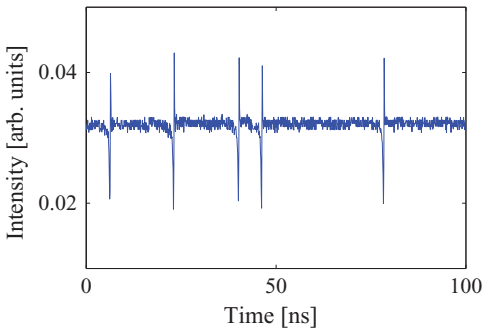

FIG. 3. (Color online) Experimental pulses for the quantum-dot device. The injection strength was approximately 0.05 and the detuning was approximately −1 GHz.

(the ratio of the intensity of the light from the master reaching the slave to the intensity of the slave in the injection-free case) was approximately 0.05 for Fig. 2(a). At this level single pulses were observed, as shown in Fig. 2(a), and outside the locking boundary a wave mixing signal was observed (resembling essentially a periodic train of single pulses). After the strength was increased to approximately 0.1, the nature of the pulsations became quite different, as shown in Fig. 2(b). Two "pulsations" are shown where the two events have very different intensity shapes. Outside the locking region at this level chaotic behavior was observed. After the strength was increased still further, the behavior returned to a simple single-pulse type, after which another complicated region was found. Continued increase of the injection level was found to change the locking boundary from a saddle-node to a Hopf bifurcation.

In contrast to these observations, for the quantum-dot devices only single pulses such as those shown in Fig. 3 were observed. (While we are primarily concerned here with the excitable features, we note that various other dynamical regimes were observed including bistability between locked behavior and a limit cycle and bistability between two locked solutions as reported in [3,5].)

B. Positive detuning

For completeness we also describe the observations for positive detuning. For quantum well devices it is well known that the locking boundary for positive detuning is of saddle-node type for a small region only and that for a large parameter range the positive detuning boundary is a Hopf bifurcation corresponding to the undamping of the relaxation oscillations (ROs). (In fact, this boundary can even cross the zero detuning line and so both the saddle-node (SN) and Hopf lines can be of negative detuning.) The locking region is bounded by saddle-node lines on both sides only for very low injection levels, and identifying excitability via traditional spectral and intensity techniques is very difficult at these levels due to the necessary low levels of injection. However, it was shown in [16] that, even for a positively detuned quantum well device, excitable phase slips could be observed by making use of an interferometric technique to measure the phasor of the slave laser at the requisite low injection levels. For the quantum-dot devices, excitable pulses are readily observed for positive detuning over a relatively large region because of the large area bounded on both sides by the saddle-node bifurcation. It

has been shown that it is the high damping of the relaxation oscillations in these devices that is responsible for the size of this region [4,5]. The most important qualitative feature for both device types is that the direction of rotation is reversed for positive detuning. That is, for negative detuning, rotations of $+2\pi$ are obtained, while for positive detuning, rotations of -2π are obtained.

III. RATE EQUATION MODELS

Let us now consider rate equation models for the systems. We begin with the equations for an optically injected quantum well device as used in [13,17],

$$\dot{E} = 1/2(1+i\alpha)nE + Ke^{i\Delta t} + F_r(t) + iF_i(t), \quad (2)$$

$$\dot{n} = -2\Gamma n - (1+2Bn)(|E|^2 - 1) + F_n(t), \quad (3)$$

where a dot means differentiation with respect to Ωt with Ω the RO frequency, E the electric field of the slave laser, α the linewidth enhancement factor of the slave, n the carrier density of the slave, Δ the detuning, and K the injection rate with both Δ and K dimensionless through a rescaling with Ω. Γ is a rescaled measure of the RO damping and B is the rescaled carrier lifetime. White noise is included via the $F_j(t)$ terms ($j = r$ for the real part of the electric field, $j = i$ for the imaginary part of the electric field, and $j = n$ for the carrier density). These are given by $F_j = \sqrt{2D_j}\xi_j(t)$ for the effective diffusion constants D_j and the stochastic terms $\xi_j(t)$ satisfying $\langle \xi_j(t) \rangle = 0$ and $\langle \xi_j(t), \xi_j(t') \rangle = \delta(t - t')$.

Figure 4 shows a stability mapping made by calculating Lyapunov exponents [18]. Mappings based on the largest Lyapunov exponent (LLE) for the optically injected laser system were previously found in [19]. In [18], the method was extended to also make use of the second largest Lyapunov exponent (SLLE): whenever the LLE is equal to zero the SLLE

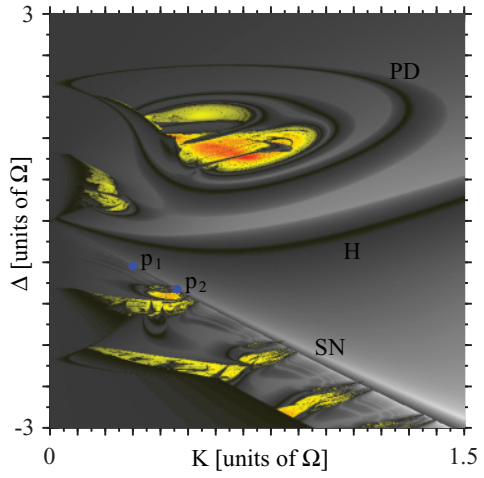

FIG. 4. (Color online) Numerical stability diagram for quantum-well equations with $\alpha = 2$, $\Gamma = 0.035$, and $B = 0.015$. Dark shading (grayscale in color version) corresponds to stable behavior while the light shading (colored in color version) corresponds to chaotic behavior. SN, H, and PD refer to saddle-node, Hopf, and period doubling bifurcations, respectively. The (blue) points p_1 and p_2 correspond to the working points for the numerical time series plots shown in Fig. 6.

is used instead. This has the advantage of providing more information about the dynamics of the system using the same computational efforts. It allows the detection of additional bifurcation curves (such as period doubling and torus bifurcations) and indicates where multistability between different limit cycles is expected to occur. Dark shading (grayscale in the color versions) corresponds to stable operation while light shading (colored in the color versions) corresponds to chaos (with red the most positive exponent). In the colored versions, black is associated with zero-value exponents. The Lyapunov figure is complementary to figures created using continuation methods, and their combination allows a fuller understanding of the dynamical behavior. In [13] a stability diagram was made using the continuation package AUTO. For comparison, we use the material parameters of [13]. The locking region for low levels of injection is bounded by a saddle-node bifurcation. For much of the saddle-node bifurcation there is a coinciding homoclinic bifurcation. The main discovery in [13] was that in certain regions the saddle-node and homoclinic bifurcations do not coincide and instead form so-called homoclinic teeth in which multipulse excitability can be found. Comparing the diagram in [13] to that here, we see that the chaotic regions just outside the locking boundary for negative detuning lie next to the homoclinic teeth. Thus, we identify the complexity of these teeth with the complex motion outside the locking boundary. The association of these chaotic regions in the unlocked region to the homoclinic teeth in the locked region does not seem to have been appreciated hitherto and may be of help in unraveling the underlying complications. While an in-depth analysis of these regions and their association to the multipulse excitability is beyond the scope of this work, a plausibility argument can be given for expecting this association. As shown in [13], there are many homoclinic tongues within a tooth and many of these either touch or come very close together. (Also, many either touch or come close to the SN line.) The behavior of the excitable trajectories within the tongues must mirror the deterministic trajectories outside them, and so where multiple homoclinic tongues are close together one expects extremely complicated dynamics. A zoom of part of the first complicated region is shown in Fig. 5, which can be compared with the corresponding continuation figure (see Fig. 3 in [13]). This supports our plausibility argument as the chaotic regions in our figure seem to grow from regions where different tongues are close together.

As was shown in [13], within the tooth the excitable response to a perturbation is deterministic, and different regions give rise to different numbers of peaks in the response. However, if noise is included then the situation is not so straightforward. The regions of different behavior can be quite small in parameter space. One effect of noise is a blurring of the boundaries between regions; that is, a noise-induced diffusion in parameter space can give rise to a distribution of the numbers of peaks in an excitable event. An example of the single-pulse behavior away from a homoclinic tooth is shown in Fig. 6(a) and that of the multipulse behavior within a tooth is shown in Fig. 6(b), showing an excellent qualitative agreement with the experimental observations. Thus, we interpret the complex regions observed experimentally as homoclinic teeth.

In [13], the importance of α in the formation of the teeth was identified. However, for multipulse excitability it is

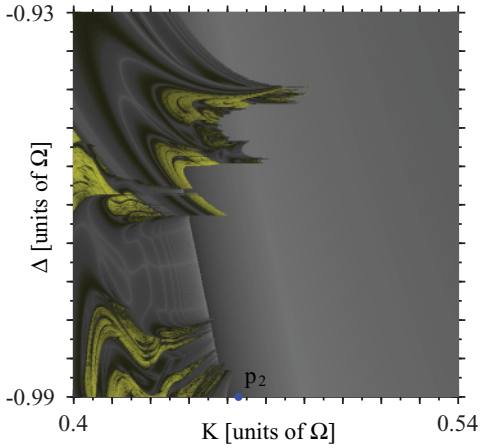

FIG. 5. (Color online) Zoom of part of Fig. 4. Dark shading (grayscale in color version) corresponds to stable behavior while the light shading (colored in color version) corresponds to chaotic behavior as in previous figures.

also necessary to have a weak RO damping. By increasing the value of the damping, the size of the chaotic regions becomes progressively smaller. Figure 7 shows the stability mapping for a higher damping value, and one can easily see the shrinking of the chaotic regions outside the homoclinic teeth. As the damping is further increased, these regions shrink further and further until for very high damping they

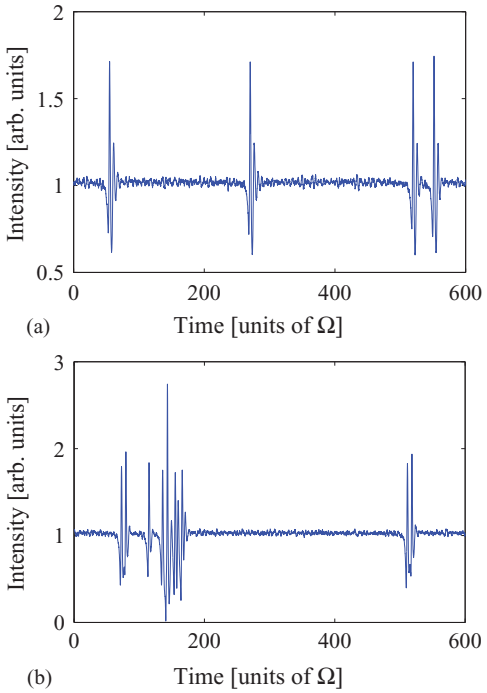

FIG. 6. (Color online) Numerical time traces for Eqs. (3). (a) An example of single-pulse excitability away from a homoclinic tooth with parameters $K = 0.3$ and $\Delta = -0.656$ (point p_1 in Fig. 4). (b) An example of multipulse excitability within a homoclinic tooth with parameters $K = 0.46$ and $\Delta = -0.99$ (point p_2 in Figs. 4 and 5). The noise parameters are $D_r = D_i = 2 \times 10^{-4}$ and $D_n = 2 \times 10^{-6}$. In the noise-free deterministic case, the parameters for (b) are in a region of double pulse excitability.

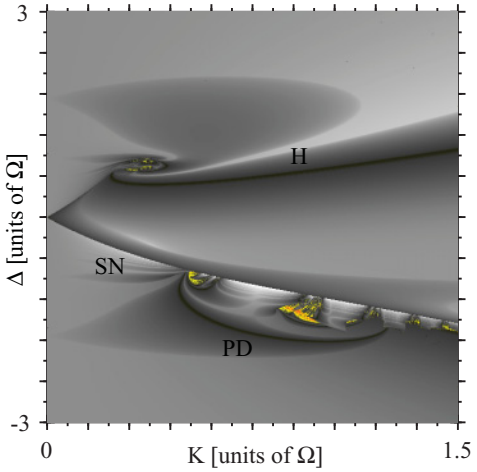

FIG. 7. (Color online) Numerical stability diagram for quantum-well equations with $\alpha = 2$, $\Gamma = 0.5$ and $B = 0.48$. SN, H and PD refer to saddle-node, Hopf and period doubling bifurcations respectively. Again, dark shadings (grayscale in color version) correspond to stable behavior while the light shadings (colored in color version) correspond to chaotic behavior.

do not appear at all. The reason why is clear. For very high damping, one may adiabatically eliminate the carrier equation in the Class A approximation. Thus, the highly damped system is effectively two-dimensional and cannot produce deterministic chaos. Even so, the separation of the saddle-node and homoclinic bifurcations persists, but for sufficiently high damping it does not lead to multipulse excitability. Rather, it can lead to a bistability between phase-locked operation and the wave-mixing limit cycle. This bistability is also observed for the quantum-dot case, as we see below.

A rate equation model for optically injected quantum-dot lasers was considered in [5]. There a four-dimensional system was considered; two equations for the electric field of the slave, one for the dot occupation probability and one for the carrier density in the wetting layer. Because of the material parameters of quantum dots operating around 1.3 μm, the occupation probability ρ of the dots is close to 1. This motivates the introduction of a small parameter ε such that $\rho = 1 + \varepsilon u$. The equation for ρ then becomes an equation for u and an adiabatic elimination of this equation can be justified (see [5] for details), bringing the system to a three-dimensional form. These equations were not explicitly given in [5], but we display them here:

$$\dot{E} = \frac{1}{2}(1 + i\alpha)\left[1 - \frac{2(1 + |E|^2)}{B\varepsilon n}\right]E + Ke^{i\Delta s}, \qquad (4)$$

$$\dot{n} = \varepsilon^{-1}\eta[J - n - 2(1 + |E|^2)]. \qquad (5)$$

In these equations, a dot means differentiation with respect to $s = \varepsilon t/\tau_{\rm ph}$; J is the pumping current; n is the carrier density in the wetting layer; $B \equiv \tau\tau_{\rm cap}^{-1}$ and $\eta \equiv \tau_{\rm ph}\tau^{-1}$, where τ, $\tau_{\rm cap}$, and $\tau_{\rm ph}$ denote the carrier recombination time, the capture time from the wetting layer to the dot, and the photon lifetime, respectively; K is the injection rate rescaled using $\varepsilon/\tau_{\rm ph}$ and Δ is the detuning, also rescaled using $\varepsilon/\tau_{\rm ph}$. Let us consider the injection-free system: this is given by simply removing the

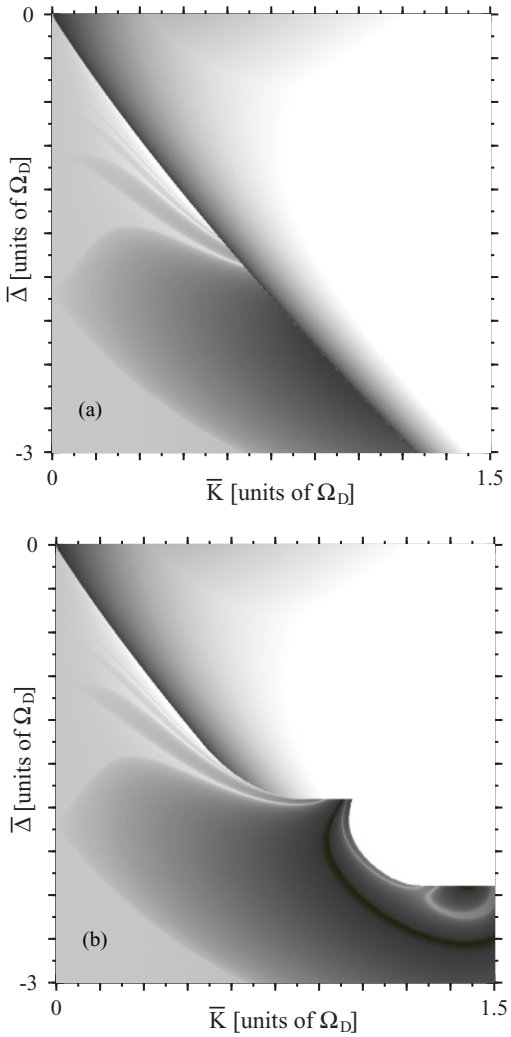

FIG. 8. (Color online) Numerical stability diagrams for the quantum-dot rate equations. The parameters are $B = 100$, $\varepsilon = 0.01$, and $J = 1.5J_{\rm th}(J_{\rm th} = 4)$ as given in [5], and we take $\alpha = 2$ as with the quantum-well case; $\bar{K} = K/\Omega_D$ and $\bar{\Delta} = \Delta/\Omega_D$. (a) Diagram generated by scanning from right to left, showing the saddle-node bifurcation clearly. (b) Diagram generated by scanning from left to right, showing clearly the separation of the saddle-node and homoclinic bifurcations.

last term in Eq. (4). A standard linear stability analysis yields the characteristic equation

$$\lambda^2 + 2\Gamma_D\lambda + \omega_0^2 = 0, \tag{6}$$

where $\Gamma_D = \frac{1}{2}(d + 1 - J_{\rm th}/J)$ and $\omega_0^2 = d(1 + B_1)[1 - J_{\rm th}/J]$ with $J_{\rm th}$ the threshold current, $B_1 \equiv B\varepsilon$, and $d \equiv \varepsilon^{-1}\eta$. Γ_D is the RO damping and the RO frequency is given by $\Omega_D^2 = \omega_0^2 - \Gamma_D^2$. Using the parameters in [5], ω_0, Γ_D, and Ω_D are comparable and, in particular, the ratio Γ_D/Ω_D is very high in comparison to that obtained for quantum well devices, as previously reported in [20,21]. This feature is responsible for many of the unique properties reported for quantum-dot lasers: it explains their enhanced stability when undergoing external optical feedback [22], it allows an enhanced stability in mutually coupled configurations [14,23], and it is also key to various properties of the optically injected quantum-dot laser described in [3–5]. In Fig. 8, the stability close to the negative detuning unlocking boundary is shown via a calculation of the Lyapunov exponents. (We take $\alpha = 2$ as in the quantum-well case, emphasizing that it is the high damping that provides the contrast rather than a low value of α. We take the other parameters from [5].) Figure 8(a) was generated by scanning from top to bottom (i.e., decreasing the detuning). Only part of the unlocking (saddle-node) boundary for negative detuning is shown. The regions of chaos identified with the homoclinic teeth for the quantum-well-based devices are not observed. Figure 8(b) was generated by increasing the detuning. When comparing the two figures, there is a clear hysteretic effect on the stability diagram (near $\bar{K} \gtrsim 0.5$ in the figure), where the saddle-node bifurcation does not coincide with the death of the unlocked, limit-cycle behavior. The details of this region are complex and deserve further study but for the purposes of this work we note that, rather than multipulse excitability, bistability between phase-locked operation and a limit cycle is observed. There are in fact (at least) two mechanisms leading to bistability in the optically injected quantum-dot system, and both are found to occur. One results from the separation of the saddle-node and homoclinic bifurcations and, indeed, this separation of the saddle-node and homoclinic bifurcations was recently predicted and demonstrated for a quantum-dot laser in [24]. The other results from the interaction of the saddle-node bifurcation and a Hopf bifurcation, as for the bistability identified in [5].

Future work may include an experimental examination of the statistics of the interpulse times. This has been considered both experimentally and theoretically for quantum-dot devices in [24]. However, thus far it has only been considered theoretically for quantum-well-based lasers in [17] and the experimental confirmation or otherwise of the results should be pursued.

IV. CONCLUSION

In conclusion, we have shown that while the appearance of excitability in an optically injected semiconductor laser is a generic feature, the manifestation of the effect can vary depending on the type of laser. Quantum-well lasers display regions of single-pulse excitability and also homoclinic teeth where very complicated multipulse trajectories are found. In contrast, highly damped quantum-dot devices display only very simple pulse trajectories. It was shown that a homoclinic tooth inducing multipulse excitability inside the locking boundary is typically associated with a chaotic region outside the locking boundary. The enhanced RO damping of quantum-dot lasers results in the removal of these chaotic regions and the associated multipulse excitability.

ACKNOWLEDGMENTS

B.K. gratefully acknowledges David Goulding, Evgeny Viktorov, and Thomas Erneux for discussions. This research was enabled by the Higher Education Authority Program for Research in Third Level Institutions (2007–2011) via the INSPIRE programme, and the authors also gratefully acknowledge the support of Science Foundation Ireland under Contract No. 07/IN.1/I929.

[1] B. Lindner, J. Garcia-Ojalvo, A. Neiman, and L. Schimansky-Geier, Phys. Rep. **392**, 321 (2004).
[2] S. Wieczorek, B. Krauskopf, T. B. Simpson, and D. Lenstra, Phys. Rep. **416**, 1 (2005).
[3] D. Goulding, S. P. Hegarty, O. Rasskazov, S. Melnik, M. Hartnett, G. Greene, J. G. McInerney, D. Rachinskii, and G. Huyet, Phys. Rev. Lett. **98**, 153903 (2007).
[4] B. Kelleher *et al.*, Opt. Lett. **34**, 440 (2009).
[5] T. Erneux, E. A. Viktorov, B. Kelleher, D. Goulding, S. P. Hegarty, and G. Huyet, Opt. Lett. **35**, 937 (2010).
[6] L. Olejniczak, K. Panajotov, H. Thienpont, and M. Sciamanna, Phys. Rev. A **82**, 023807 (2010).
[7] F. Plaza, M. G. Velarde, F. T. Arecchi, S. Boccaletti, M. Ciofini, and R. Meucci, Europhys. Lett. **38**, 85 (1997).
[8] M. Giudici, C. Green, G. Giacomelli, U. Nespolo, and J. R. Tredicce, Phys. Rev. E **55**, 6414 (1997).
[9] H. J. Wünsche, O. Brox, M. Radziunas, and F. Henneberger, Phys. Rev. Lett. **88**, 023901 (2001).
[10] S. Beri, L. Marshall, L. Gelens, G. Van der Sande, G. Mezosi, M. Sorel, J. Danckaert, and G. Verschaffelt, Phys. Lett. A **374**, 739 (2010).
[11] S. Wieczorek, T. B. Simpson, B. Krauskopf, and D. Lenstra, Phys. Rev. E **65**, 045207 (2002).
[12] R. Adler, Proc. IEEE **61**, 1380 (1973).
[13] S. Wieczorek, B. Krauskopf, and D. Lenstra, Phys. Rev. Lett. **88**, 063901 (2002).
[14] B. Kelleher, C. Bonatto, P. Skoda, S. P. Hegarty, and G. Huyet, Phys. Rev. E **81**, 036204 (2010).
[15] B. Kelly *et al.*, Electron. Lett. **43**, 1282 (2007).
[16] B. Kelleher, D. Goulding, B. Baselga-Pascual, S. P. Hegarty, and G. Huyet, Eur. Phys. J. D **58**, 175 (2010).
[17] S. Wieczorek and D. Lenstra, Phys. Rev. E **69**, 016218 (2004).
[18] C. Bonatto, J. C. Garreau, and J. A. C. Gallas, Phys. Rev. Lett. **95**, 143905 (2005).
[19] K. E. Chlouverakis and M. J. Adams, Opt. Commun. **216**, 405 (2003).
[20] T. Erneux, E. A. Viktorov, and P. Mandel, Phys. Rev. A **76**, 023819 (2007).
[21] M. Kuntz, N. N. Ledentsov, D. Bimberg, A. R. Kovsh, V. M. Ustinov, A. E. Zhukov, and Yu. M. Shernyakov, Appl. Phys. Lett. **81**, 3846 (2002); K. Lüdge, M. J. P. Bormann, E. Malić, P. Hövel, M. Kuntz, D. Bimberg, A. Knorr, and E. Schöll, Phys. Rev. B **78**, 035316 (2008).
[22] D. O'Brien *et al.*, Electron. Lett. **39**, 1819 (2003); D. O'Brien, S. P. Hegarty, G. Huyet, and A. V. Uskov, Opt. Lett. **29**, 1072 (2004).
[23] S. P. Hegarty, D. Goulding, B. Kelleher, G. Huyet, M.-T. Todaro, A. Salhi, A. Passaseo, and M. De Vittorio, Opt. Lett. **32**, 3245 (2007).
[24] B. Kelleher, D. Goulding, G. Huyet, E. Viktorov, T. Erneux, and S. P. Hegarty (unpublished).